

Electron Ionization Dynamics of SF₆

James N Bull^a, Jason W L Lee^b, Claire Vallance^{b,†}

^a School of Chemistry, University of Melbourne, Parkville VIC 3010, Melbourne, Australia. Email: james.bull@eigenket.org

^b Chemistry Research Laboratory, Department of Chemistry, University of Oxford, 12 Mansfield Road, Oxford OX1 3TA, United Kingdom

[†]Corresponding author: E-Mail: claire.vallance@chem.ox.ac.uk

A detailed understanding of the dissociative electron ionization dynamics of SF₆ is important in the modelling and tuning of dry-etching plasmas used in the semiconductor manufacture industry. This paper reports a crossed-beam electron ionization velocity-map imaging study on the dissociative ionization of cold SF₆ molecules, providing the first complete, unbiased kinetic energy distributions for all significant product ions. Analysis of these distributions suggest that fragmentation following single ionization proceeds *via* formation of SF₅⁺/SF₃⁺ ions that then dissociate further in a statistical manner through loss of F atoms or F₂, until most internal energy has been liberated. Similarly, formation of stable dications is consistent with initial formation of SF₄²⁺ ions, which then undergo further dissociation on a longer timescale. The present study provides the first opportunity to perform a detailed comparison between electron ionization and photoionization dynamics for a ‘large’ polyatomic molecule, revealing similar dynamical behaviour. In parallel with the ion kinetic energy distributions, the velocity-map imaging approach provides a new set of partial ionization cross-sections for all detected ionic fragments over an electron energy range of 50 – 100 eV, providing the first recorded partial cross-sections for S²⁺, and enable the cross-sections for SF₄²⁺ from SF⁺ to be resolved.

PACS number(s): 06.30.Gv, 34.80.Ht, 34.80.Gs

I. INTRODUCTION

Sulphur hexafluoride, SF₆, is widely used as a gas-phase dielectric medium in high-voltage electronics and as an etchant precursor in semiconductor manufacture [1-6]. In order to model and tune etching processes, quantitative information on the fundamental collision physics is needed. Useful quantities in this context include ion threshold energetics, formation cross-sections, ion kinetic energies associated with dissociation, and knowledge of product electronic states. For example, fluorine atoms produced in dry-etching plasmas penetrate into silicon wafer substrates to form SiF_n ($n = 1 - 4$), with the penetration distance depending on the velocity of the fluorine atoms. Further etching processes can be induced through application of electrical potentials to the substrate, promoting ion bombardment etching.

Because the chemistry and physics of dry-etching plasmas involves electron-molecule collisions leading to ionization and dissociation, there is a clear need for reliable partial ionization cross-sections and associated ion kinetic energy distributions for etchant gases such as SF₆. While a large number of electron ionization cross-sections have been reported for SF₆, summarised in a number of reviews [2,7,8], there is varying agreement between the different determinations. This variation is due partly to the fact that conventional mass spectrometers and weak-field ion sources with small source apertures discriminate against ions formed with high kinetic energy [9,10]. It is now well-established that SF₆, like other small saturated perfluorinated species, does not have a bound parent cation in the Franck-Condon window. Ionization therefore leads to impulsive or prompt dissociation, yielding fragment ions with high kinetic energy [11,12]. Consequently, fragment kinetic energy distributions contain important information on the dissociation dynamics. However, there is a distinct lack of complete, unbiased ion kinetic energy distributions for feedstock molecules relevant in plasma etching processes. While kinetic energy distributions for electron ionization of SF₆ have been reported for a few of the possible ion fragments [13], the retarding potential method used for these measurements is generally unreliable, and can suffer large biases against ions of certain energies depending on the detailed experiment design and implementation. Overall, there is a clear

need for reliable ion kinetic energy distributions associated with dissociative ionization of SF₆.

Gaining a detailed understanding of the microscopic dynamics of electron ionization for a ‘large’ molecular target like SF₆ is a challenging task due to the array of possible ionized states that may be accessed [10,14]. Electron ionization is a collisional interaction, in which the electron may in principal transfer any fraction of its kinetic energy to the molecule. However, usually only a relatively modest fraction of the energy is transferred, and, because the collision is fast compared with nuclear rearrangement, usually a vertical excitation is invoked [14]. For example, the electron energy loss spectrum for SF₆ shows a broad distribution in the 10 – 50 eV kinetic energy loss range, with three clear peaks consistent with the first few electronic states of SF₆⁺, and an autoionizing shape resonance converging with the E²T_{1u} state of SF₆⁺ [15, 16]. Photoelectron spectroscopy has shown the ground and first three excited states of SF₆⁺ to be repulsive [16], consistent with the expectation of impulsive dissociation.

This paper reports a velocity-map imaging study on the electron ionization of jet-cooled SF₆ molecules. Velocity-map imaging offers the clear advantage over previous techniques of yielding high-resolution ion kinetic energy distributions, particularly for ions with less than 1 eV kinetic energy [17-19]. The measured kinetic energy distributions suggest that electron-impact-induced single dissociative ionization leads to impulsive production of SF₅⁺ and SF₃⁺ ions, which then dissociate statistically over much longer timescales *via* loss of fluorine atoms and/or molecular fluorine, F₂. This combination of electron ionization dynamics is likely to be common to other saturated perfluorocarbon species. Comparison of the fragment ion kinetic energy distributions recorded in the present work with available mean kinetic energies extracted from threshold photoelectron-photoion coincidence (TPEPICO) provides the first clear demonstration of the similarity between electron-induced and photon-induced fragmentation for a ‘large’ polyatomic molecule.

II. EXPERIMENTAL METHODS

Measurements were performed using two electron ionization

instruments: (i) absolute total ionization cross-section measurements were performed using a purpose-built apparatus designed to have unit ion detection efficiency [20]; and (ii) ion kinetic energy distributions and partial ionization cross-sections were recorded using a velocity-map imaging apparatus [18].

The total ionization cross-section instrument, described in detail previously [20], utilizes a magnetically collimated electron beam and an ion collector surface that surrounds the interaction region to achieve unit ion detection efficiency, irrespective of ion kinetic energy. The electron energy scale was calibrated by extrapolating the total ionization efficiency curve for pure argon to the known ionization energy [21]. The instrumental uncertainty in the measured cross-sections is estimated to be $\pm 4\%$. The reported total ionization cross-section curve is the average of eight separate experimental runs, all of which are within the $\pm 4\%$ instrumental error.

The velocity-map imaging instrument has been described in detail previously [18]. For the present measurements, SF_6 was prepared in a supersonic molecular beam by admitting $\sim 180 \mu\text{s}$ pulses into the instrument *via* a Parker Hannifin Corp. Series 9 pulsed solenoid valve (background pressure $\sim 2 \times 10^{-7}$ Torr). After passing through a 1 mm diameter skimmer, the molecular beam pulse was crossed with an electron pulse of ~ 30 ns duration with a selected electron energy (~ 0.25 eV FWHM resolution). The electron pulses were produced from a modified PSP Vacuum ELS100 electron gun employing a LaB₆ single-crystal thermionic emission source. The two beams crossed within a set of velocity-mapping ion optics, which were initially held at ground potential. As soon as the electron pulse had cleared the interaction region on each experimental cycle, the velocity-mapping electrodes were switched from ground to the optimised velocity-mapping potentials using a pair of high-voltage Behlke switches. The potentials applied to the velocity-mapping electrodes allowed imaging of ions formed with kinetic energies up to 12 eV. The velocity-mapped ions were detected using a Photonis dual 40 mm chevron-mounted MCPs and P47 phosphor assembly. Images produced on the phosphor were captured by a Photonic Science MiniFDI intensified CCD camera, time-gated to the arrival time of the ion of interest, and the total (time-dependent) signal at the phosphor was monitored by a fast photomultiplier (Hamamatsu H10721-01), providing time-of-flight spectra of all ions. Time-of-flight spectra recorded as a function of electron energy allowed the partial ionization cross-sections for each fragment ion to be determined. The repetition rate of the experiment was ~ 15 Hz, limited by the acquisition speed of the CCD camera.

Partial ionization cross-sections were recorded in the electron energy range from 50 to 100 eV in 2.5 eV increments. Velocity-map images were recorded for SF_5^+ , SF_4^+ , SF_3^+ , SF_2^+ , SF^+ , S^+ and F^+ ions with 60 eV, 80 eV, and 100 eV incident electrons, from which fragment kinetic energy distributions were extracted. Images for the doubly-charged ions SF_4^{2+} , SF_3^{2+} and SF_2^{2+} were recorded with 100 eV electrons. Images for SF_5^+ were accumulated over 100,000 acquisition cycles, while all other images were accumulated over 1,000,000 acquisition cycles. Each image was processed on-the-fly using in-house-developed thresholding and centroiding algorithms [22], and was background-corrected post acquisition by subtracting an image for which the electron pulse was timed to clear the interaction volume shortly before arrival of the molecular beam.

Velocity-map images were reconstructed to determine the centre-of-mass velocity and angular distributions using a polar onion peeling (POP) algorithm [23]. All angular distributions were found to be isotropic, corresponding to no preferential alignment of any dissociation axes relative to the (unpolarised) electron beam propagation direction [18,24]. The velocity-to-

kinetic energy scale was calibrated from the known kinetic energy distribution of N^+ ions formed in the electron ionization of N_2 at 100 eV [18].

III. RESULTS AND DISCUSSION

A. Total and partial electron ionization cross-sections

Although the main focus of the present study is high-quality ion kinetic energy distributions, we also recorded total and partial ionization cross-sections. The total ionization cross-section is shown in FIG. 1 and is in excellent agreement with the measurement of Rejoub *et al.* [25] (see Supplemental Material [26] for numerical tabulation). Partial ionization cross-sections, normalized to the total ionization cross-section are shown in FIG. 2 (see Supplemental Material [26] for numerical tabulation). The partial ionization cross-sections recorded for SF_5^+ , SF_4^+ , SF_3^+ , SF_2^+ , S^+ , F^+ , SF_3^{2+} , SF_2^{2+} , and SF^{2+} are in good agreement with the data of Rejoub *et al.* [25], recorded at a lower resolution of 10 eV increments. The higher mass resolution of our study allowed the cross-sections for the SF^+ and SF_4^{2+} ions to be resolved from one another, though we note that their combined partial ionization cross-section is in good agreement with Rejoub *et al.* [25]. In addition, we provide the first measured partial ionization cross-section for production of S^{2+} . Our measurements differ from Rejoub *et al.* [25] in that their instrument was able to measure absolute partial ionization cross-sections, which were then summed to yield the total ionization cross-section. In contrast, in the present experiment it is difficult to characterise any small changes in the electron beam flux or focusing conditions as a function of electron energy due to the open-architecture geometry of the ionization zone required for velocity-map imaging. As a consequence, relative partial ionization cross-sections are recorded, which are then normalized to the independent absolute total ionization cross-section. Note that because velocity-map imaging maps all ions formed within a finite-sized ionization volume but with the same velocity vector to the same point on the position sensitive detector, any variation in spatial overlap or interaction density between the electron beam and molecular beam will not have a significant bearing on the results [17].

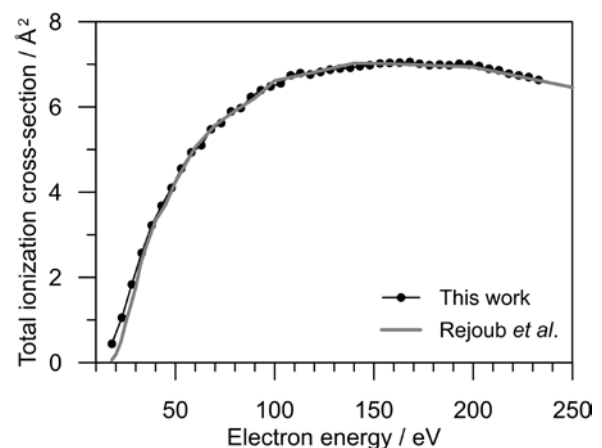


FIG. 1 – Total ionization cross-sections for electron ionization of SF_6 . Rejoub *et al.* from Ref. [25]. Total ionization cross-section values at intermediate energies can be obtained through interpolation with a high-order polynomial.

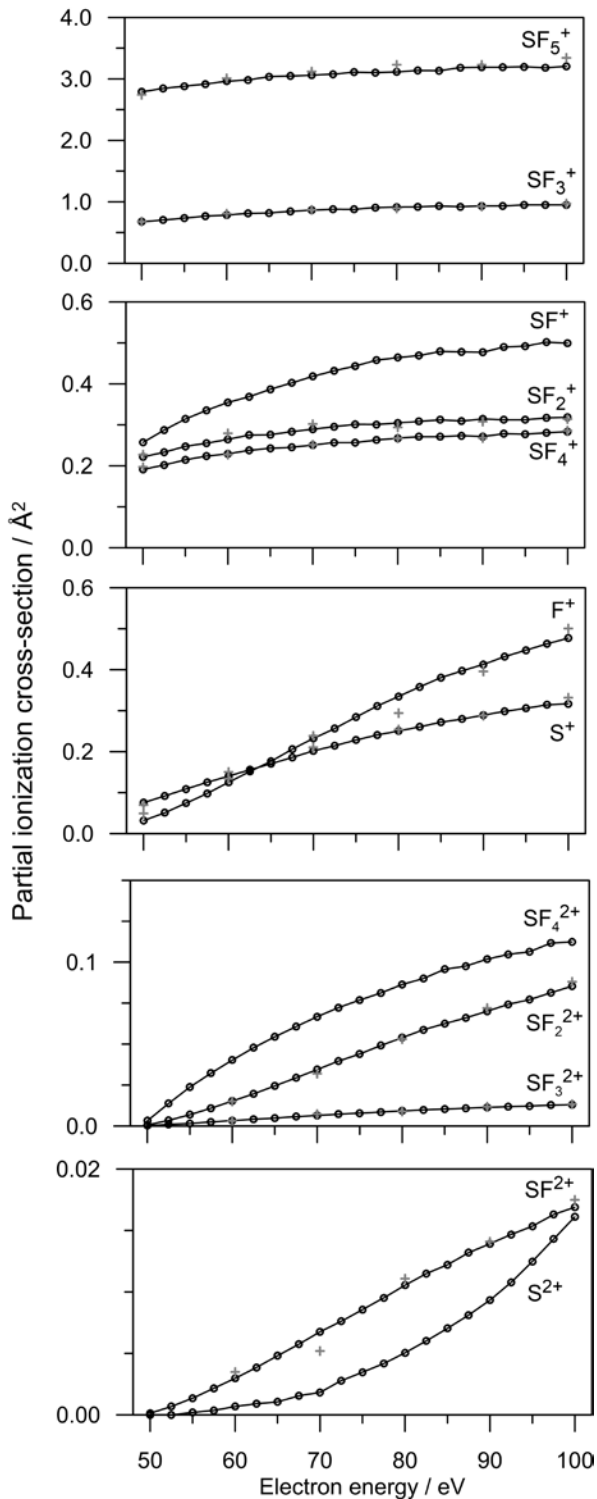


FIG. 2 – Partial ionization cross-sections for electron ionization of SF_6 . Grey crosses at 10 eV intervals are values from Rejoub *et al.* [25]; SF^+ , SF_4^{2+} and S^{2+} channels have not been resolved previously.

B. Kinetic energy distributions for monocations

Kinetic energy distributions for SF_n^+ ($n = 0 - 5$) ions recorded at 100 eV are shown in FIG. 3. From the partial ionization cross-

sections shown in FIG. 2 and the ion-pair double ionization cross-sections reported in Rejoub *et al.* [25], we can surmise that the $n = 2 - 5$ ions giving rise to these distributions arise predominantly from single ionization processes. The SF^+ , S^+ and F^+ ion signals, however, are likely to have significant contributions from double ionization processes that lead to the production of ion pairs.

SF_5^+

SF_5^+ , which is the predominant product at all electron energies, has a skewed Gaussian kinetic energy distribution peaking at 0.14 eV. The distribution is consistent with impulsive dissociation along one or more repulsive potential energy surfaces (in contrast, a ‘statistical’ dissociation occurring over long timescales would produce a Boltzmann-like kinetic energy distribution peaking near zero kinetic energy – see examples in Ref. [17]).

Conservation of momentum would imply that the partner fluorine atom is formed with a kinetic energy distribution peaking at 0.80 eV. Supporting IP-EOM-CCSD calculations reported in the Supplemental Material [26] predict that the first two dissociation curves of SF_6^+ produce ground state $\text{SF}_5^+ + \text{F}$, with asymptotic mean ion kinetic energy for SF_5^+ of 0.14 eV and 0.59 eV, respectively. These calculations are consistent with the experimental observations.

The measured SF_5^+ kinetic energy distribution compares favourably with mean ion kinetic energies obtained from TPEPICO measurements on SF_6 [12]. These show the first two photoelectron bands (X^2T_{1g} and $\text{A}^2\text{T}_{1u} + \text{B}^2\text{T}_{2u}$) to be intense and to yield exclusively SF_5^+ with mean ion kinetic energy of ~0.13 eV and ~0.13 – 0.29 eV, respectively. Note that the literature TPEPICO measurements do not provide a high-resolution ion kinetic energy distribution, only a mean ion kinetic energy. The C^2E_g state, which is unclear in the electron energy loss spectra, predominantly yields SF_5^+ with a mean ion kinetic energy of 0.2 eV; the D^2T_{2g} state produces minor quantities of SF_5^+ . In addition, other velocity-map photoion imaging measurements and rotatable detector measurements over the first four bands show strongly anisotropic images and ion kinetic energies (0.1 – 0.2 eV) independent of the exact excitation energy [27,28]. An anisotropic distribution is surprising for an octahedral molecule, and can be explained in terms of significant contributions from short-lived autoionizing resonances of neutral SF_6 . Whatever the details of the electronic states, it is clear that electron ionization and photoionization have similar dissociative ionization dynamics. In summary, the SF_5^+ kinetic energy distribution measured in the present work is consistent with population of the X^2T_{1g} , A^2T_{1u} and B^2T_{2u} states of SF_6^+ .

SF_4^+

The kinetic energy distribution recorded for SF_4^+ fragments is very similar to that for SF_5^+ , although with two maxima at 0.13 and 0.18 eV. The TPEPICO measurements [12] revealed SF_4^+ production from the D^2T_{2g} state of SF_6^+ , with a corresponding ion kinetic energy of 0.24 eV when partnered by F_2 . Other high-resolution photoelectron studies [16] revealed vibrational structure in fragments formed following excitation to the D^2T_{2g} state, suggesting that dissociation from this state has some contribution occurring over a timescale of at least a few vibrational periods. Another set of synchrotron photoionization measurements [27] show some SF_4^+ to be produced from the C^2E_g state and *via* an autoionizing resonance converging with the E^2T_{1u} state. Because the SF_5^+ and SF_4^+ kinetic energy distributions in the present study are found to be comparable, the

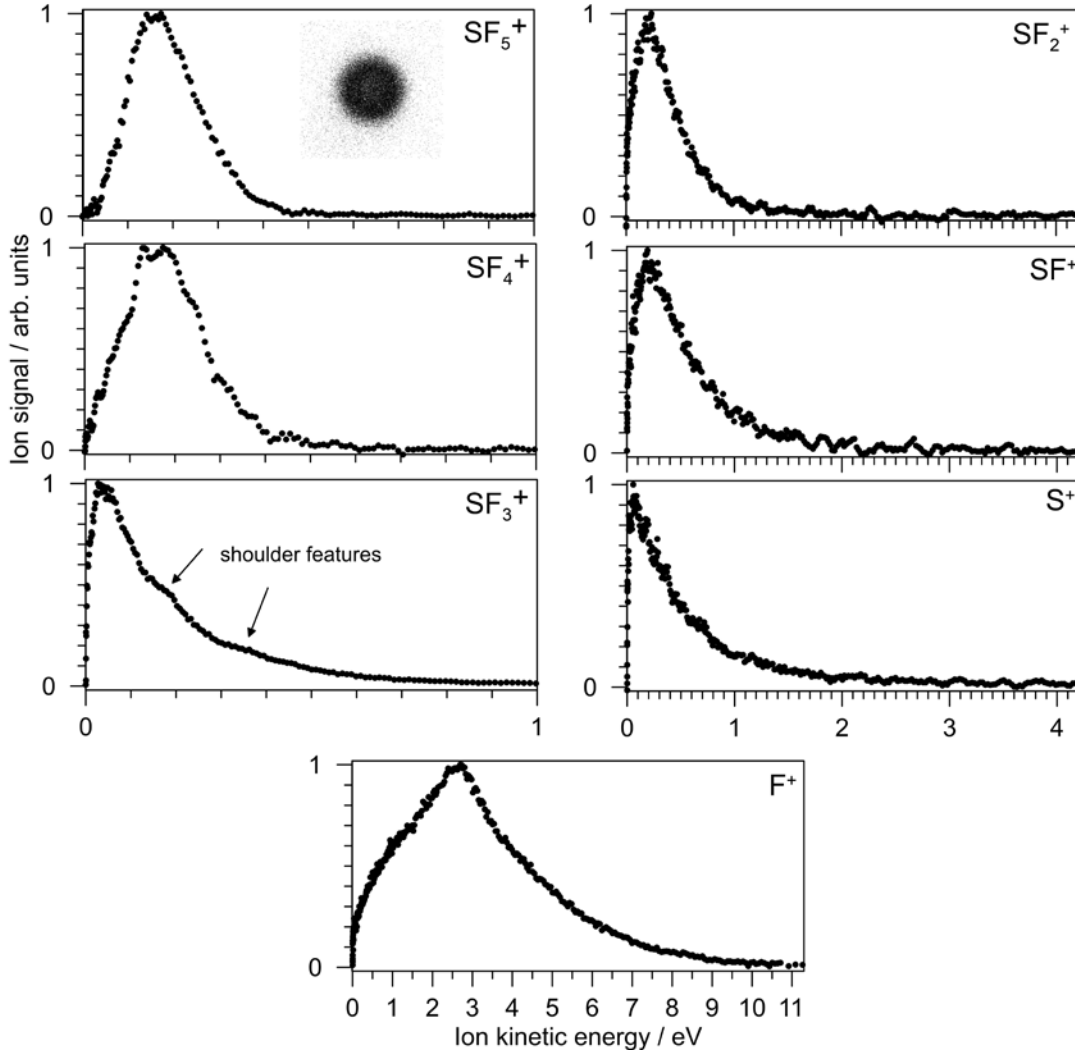


FIG. 3 – Kinetic energy distributions for singly-charged ions following 100 eV electron ionization of SF_6 . The velocity-map image for SF_5^+ is included.

electronic states involved and the subsequent dissociation dynamics are likely to be similar. Specifically, the SF_4^+ kinetic energy distribution is consistent with impulsive dissociation of nascent SF_6^+ to produce electronically excited SF_5^+ , either directly or through rapid internal conversion, followed by a statistical loss of another fluorine atom. Because a statistical dissociation following extensive redistribution of internal energy produces ions with low kinetic energy, the loss of the second fluorine atom only has a relatively small effect on the fragment kinetic energy distribution. The bimodal peak observed in the SF_4^+ kinetic energy distribution may reflect multiple secondary dissociation channels.

SF_3^+

SF_3^+ is the second most abundant ion fragment. The SF_3^+ kinetic energy distribution differs from the SF_5^+ and SF_4^+ kinetic energy distributions in that it peaks at a much lower energy of 0.03 eV with two subtle ‘shoulder’ peaks at 0.16 eV and 0.35 eV. The low energy part of the distribution is consistent with a longer timescale statistical dissociation, an interesting result considering

that the ground state of SF_6^+ is unbound. The TPEPICO measurements show the D^2T_{2g} and E^2T_{1u} states of SF_6^+ to produce SF_3^+ with mean kinetic energies of 0.15 eV (with $\text{F} + \text{F}_2$ partner fragments) and 0.36 eV (with three atomic fluorine partners) [12], respectively, consistent with the two observed shoulder features. These features can therefore be tentatively assigned to SF_3^+ products generated in the secondary dissociation of primary SF_5^+ ions formed from two different electronic states *via* the impulsive dissociation of SF_6^+ .

The TPEPICO and other photoelectron measurements revealed the signals arising from the D^2T_{2g} and E^2T_{1u} of SF_6^+ to have vibrational structure [12,16], suggesting that some population of these states lives for a few vibrational periods or more, potentially contributing to the ‘statistical’ portion of the SF_3^+ signal. As noted in the introduction, formation of the E^2T_{1u} state of SF_6^+ is associated with an autoionizing shape resonance of SF_6 , which is clearly observed in the electron energy loss spectra, and from ion abundances is probably associated with a statistical kinetic energy distribution. Other synchrotron photodissociation measurements show SF_3^+ to be a major product over this autoionizing resonance [27]. The ‘statistical’ SF_3^+ may

result from loss of a fluorine atom or F_2 molecule on an excited state potential energy surface of SF_6^+ , followed by statistical loss of further fluorine atoms. Whatever the detailed sequence of dynamics, it is clear that multiple single ionization pathways contribute to the SF_3^+ signal, and that the autoionizing resonance has a significant bearing on the overall electron ionization dynamics of SF_6 .

The SF_3^+ ion has been considered in a number of other studies, due to an anomalous feature in both its partial electron ionization cross-section at ~ 45 eV [29-31], and in photoionization efficiency curves [32,33]. The feature has been attributed to Coulomb explosion of SF_4^{2+} precursor states, yielding the $SF_3^+ + F^+$ ion pair. While ion pair cross-sections are small compared with single ionization processes at the electron energies considered in the present study [25], the SF_3^+ kinetic energy distribution will contain a minor contribution from this channel. Further evidence for this channel can be found in a mass-analyzed ion kinetic energy spectrometry (MIKEs) study on SF_4^{2+} by Matt-Leubner *et al.* [29], a 1300 eV electron ionization ion-pair coincidence study by Bapat *et al.* [34], and photoionization dication triple coincidences observed by Eland and co-workers [35,36] and by Lange *et al.* [37]. These studies assign the channel to a deferred charge-separation mechanism whereby a low energy neutral ejection ($SF_6^{2+} \rightarrow SF_4^{2+} + F_2$), producing SF_4^{2+} with ~ 0.1 eV kinetic energy, is followed by a higher energy charge separation ($SF_4^{2+} \rightarrow SF_3^+ + F^+$), producing SF_3^+ with ~ 0.85 eV kinetic energy. We propose that the tail of the present SF_3^+ kinetic energy distribution, which extends to ~ 0.9 eV, is likely to reflect this double ionization channel.

SF_2^+ , SF^+ , S^+ and F^+

The kinetic energy distributions for SF_2^+ , SF^+ , S^+ and F^+ are difficult to interpret in detail due to the number of possible fragmentation channels. The SF_2^+ distribution peaks at 0.23 eV, and does not correspond to a statistical dissociation (and is inconsistent with ‘statistical’ SF_3^+ precursor). Because the ion pair ($SF_2^+ + F^+$) cross-section of 0.032 \AA^2 at 100 eV is small compared with the total SF_2^+ partial ionization cross-section of 0.319 \AA^2 [25], the ion kinetic energy distribution will predominantly result from single ionization processes. The tail of the distribution, extending to ~ 1.25 eV, is probably due to multiple ionization processes and Coulomb explosions. TPEPICO measurements show that SF_2^+ is produced from the E^2T_{1u} and F^2A_{1g} states of SF_6^+ [12], although the ion signal was too weak to extract mean ion kinetic energies for comparison with the present work. The present kinetic energy distribution is again consistent with formation of precursor SF_5^+/SF_3^+ followed by statistical dissociations to liberate vibrational energy in excess of the dissociation threshold.

The SF^+ kinetic energy distribution is similar to that for SF_2^+ , peaking at 0.16 eV and extending to 1.5 eV. The TPEPICO measurements show that SF^+ is produced from the F^2A_{1g} state of SF_6^+ , [12] with a small contribution from double ionization [25]. We assign SF^+ to result from further statistical dissociation of SF_2^+ .

The S^+ kinetic energy distribution peaks at 0.05 eV. The very low peak kinetic energy release for this fragment suggests that it may be formed at least in part *via* symmetric loss of fluorine atoms in a Coulomb explosion. The partial ionization cross-section measurements of Rejoub *et al.* [25] show the appearance of the S^+ ion to be correlated with the onset of double ionization, supporting the suggestion that this ion is produced *via* Coulomb explosion processes.

The kinetic energy distribution of the F^+ fragment is complex due to the large number of formation channels. There is a clear peak at 2.6 eV, a weak low energy shoulder at ~ 1.0 eV and a high energy tail extending to ~ 11 eV. Importantly, there is no peak near zero kinetic energy, showing that there is no single ionization statistical dissociation processes yielding F^+ . We note that partial ionization cross-sections and energetic threshold for production of F^+ imply that the ion is formed predominantly through double ionization processes [25,29]. PEPICO measurements with 25.6 nm radiation [36], and ion-ion coincidence studies with 1300 eV electrons, [34] and a 2 MeV He^{2+} impact study [37] all recorded mean kinetic energies for F^+ that are broadly in agreement with the present work. We conclude that the F^+ species arises from a complex combination of impulsive dissociation ($SF_5^+ + F^+$), delayed charge-separation (e.g. $SF_3^+ + F^+$) and Coulomb explosion (e.g. $S^+ + F^+$) dynamics.

C. Kinetic energy distributions for dications

The kinetic energy distributions for the detected dications, SF_4^{2+} , SF_3^{2+} , and SF_2^{2+} , which must result from double ionization processes, are shown in FIG. 4. While the partial ionization cross-section measurements (time-of-flight spectra) showed trace yields of SF_2^{2+} and S^{2+} , the signals were too weak to allow velocity-map images to be recorded. Interestingly, SF_5^{2+} was not observed in the time-of-flight spectra, suggesting it has no stable states accessible through electron ionization. Double ionization in electron-molecule collisions generally results from Auger mechanisms following ionization of a core electron [38]. The nascent SF_6^{2+} species can dissociate to yield either a secondary dication and a neutral or an ion pair. Synchrotron spectroscopy measurements [39,40] have shown the SF_6 double ionization

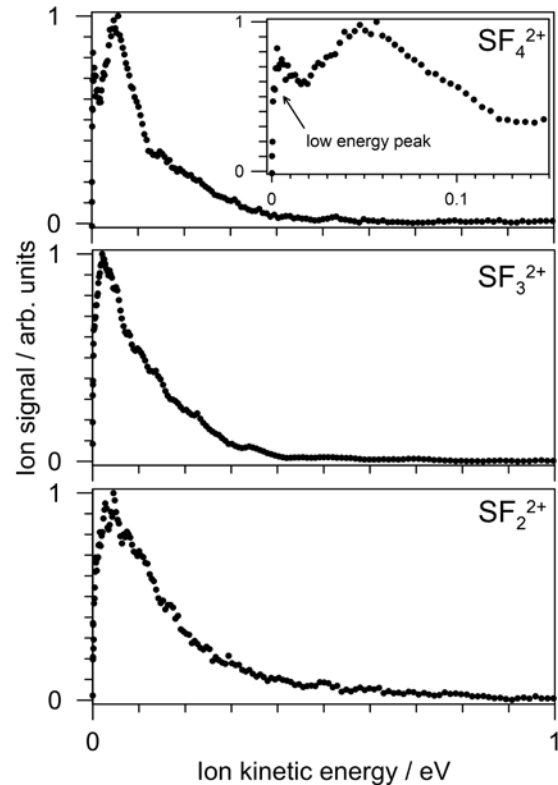


FIG. 4 – Kinetic energy release distributions for doubly-charged ion products from the 100 eV electron ionization of SF_6 .

region to lie in the energy range from 30 – 50 eV, and revealed multiple and overlapping electronic states of SF_5^{2+} and autoionizing Rydberg states.

The SF_4^{2+} kinetic energy distribution has three features, a very low kinetic energy peak at 3 meV (see zoomed inset), the main peak at 0.55 eV, and a broad shoulder between 0.14 and 0.5 eV. The peak at 3 meV is consistent with the expected thermal energy of SF_6 molecules in the molecular beam [18], thus suggesting the assignment of this feature to impulsive (and concerted) dissociation of two opposed fluorine atoms from SF_6^{2+} . The other two features in the kinetic energy distribution probably result from loss of two adjacent fluorine atoms from other repulsive electronic states of SF_6^{2+} ; because SF_5^{2+} is not stable, SF_4^{2+} cannot be produced through a statistical dissociation process. Dissociation of hot SF_4^{2+} may contribute to the deferred charge separation $\text{SF}_3^+ + \text{F}^+$ channel noted earlier [35, 36].

The SF_3^{2+} and SF_2^{2+} kinetic energy distributions are statistical in appearance, peaking at 0.02 eV and 0.04 eV, respectively. We propose that these two ions are formed statistically from SF_4^{2+} following population of higher excited states of SF_6^{2+} .

D. 60 eV and 80 eV electron energies

The data discussed so far were all acquired at an electron kinetic energy of 100 eV. Kinetic energy distributions for SF_n^+ ($n = 0 - 5$) and F^+ recorded with 60 eV and 80 eV electron energies are found to be essentially identical to those recorded at 100 eV. The invariance of the kinetic energy distributions with electron energy contrasts with the N^+ kinetic energy distributions observed in the electron ionization of N_2 [18], in which the distribution changes considerably over the 60 – 100 eV electron energy range due to increasing contributions of higher-lying electronic states of N_2^{2+} . For SF_6 , the result suggests there are no significant changes in dissociative ionization dynamics over the 60 – 100 eV electron energy range. The fact that the major ions have similar partial ionization cross-sections over this energy range also suggests that there are no significant changes in nascent electronic state populations. The minor exception is S^{2+} , the production of which is probably associated with triple ionization.

E. Comparison with retarding potential measurements

It was noted in the introduction that there has been a previous report of kinetic energy distributions for SF_n^+ ($n = 1 - 5$) using a retarding potential apparatus combined with a magnetic sector mass filter [13]. While the present SF_5^+ distribution broadly agrees with the earlier measurement, the distributions for the other ions are in very poor agreement albeit they were recorded with an electron energy of 45 eV. Specifically, for SF_n^+ ($n = 1 - 4$), all retarding potential kinetic energy distributions have a similar distribution peaking somewhere in the 0.8 – 1.1 eV range. The reason for the disagreement is unclear; we speculate the design of the retarding potential apparatus perturbed the nascent kinetic energy distribution.

As a final comparison, the F^+ kinetic energy distribution at 100 eV recorded in the present work is in agreement with the low-resolution measurements of Pullen and Stockdale [41], showing a peak at 2.8 eV and a tail extending to ~10 eV. The instrument of Pullen and Stockdale was unable to record the kinetic energy distribution below ~1 eV. Overall, it is clear that velocity-map imaging provides a higher resolution approach for measuring the entire kinetic energy distribution.

F. Electron ionization and photoionization dynamics

The kinetic energy distributions for SF_n^+ ($n = 3 - 5$) recorded in the present work agreed with mean ion kinetic energies for several product ions from TPEPICO measurements, which probe particular electronic states of SF_6^+ . The earlier photoionization measurements provide only mean ion kinetic energies for a few of the product ions, in contrast to the full, non-Gaussian and structured ion kinetic energy distributions recorded in the present study for ten ion products. The agreement found with the present electron ionization kinetic energy distributions suggests (i) the impacting electron only transfers a small amount of its kinetic energy and directly populates the same states as photoionization, a contention in part supported by electron energy loss spectroscopy, or (ii) if the impacting electron populates a variety of states not accessed in photoionization, these states quickly internally convert to a common set of dissociating states. We suspect both mechanisms are active for SF_6 . For example, as noted above in the SF_5^+ section, synchrotron velocity-map imaging measurements [27] revealed the kinetic energy distribution to be invariant across the first few electronic states of SF_6^+ , supporting a common dissociative state.

IV. CONCLUSIONS

In summary, kinetic energy distributions for the most abundant ion products resulting from electron ionization of SF_6 with 60 – 100 eV electrons have been recorded. The distributions are consistent with impulsive formation of SF_5^+ and SF_3^+ , followed by statistical loss of further fluorine atoms or F_2 until internal energy in excess of the relevant dissociation thresholds has been liberated. Similarly, stable dications appear to result from formation of SF_4^{2+} precursor ions followed by statistical dissociation. Overall, it is clear that numerous excited states of SF_6 , SF_6^+ and SF_6^{2+} play a role in the observed fragmentation. The kinetic energy distributions recorded for SF_n^+ ($n = 0 - 5$) and F^+ at electron energies of 60 and 80 eV are essentially identical to those recorded at 100 eV, suggesting that similar dissociative ionization dynamics occur across this range of electron energies.

The kinetic energy distributions for singly-charged ions recorded in the present work have been compared with TPEPICO measurements, which provide mean ion kinetic energies associated with particular electronic states of SF_6^+ . In all cases there is good agreement, suggesting that both ionization methods access similar excited states and/or fast internal conversion populates a common set of dissociative states. We are unaware of any similar comparisons between electron ionization and photoionization for a polyatomic molecule.

ACKNOWLEDGEMENTS

Funding is acknowledged from the EPSRC Programme Grants EP/G00224X/1 and EP/L005913/1, from the Marie Curie Initial Training Network 238671 ‘ICONIC’, and from ERC Starting Independent Research Grant 200733.

- [1] L. G. Christophorou and J. K. Olthoff, *Fundamental Electron Interactions with Plasma Processing Gases*, Kluwer Academic/Plenum Publishers, New York, 2004.
- [2] L. G. Christophorou and J. K. Olthoff, *J. Phys. Chem. Ref. Data* **29**, 267 (2000).
- [3] V. M. Donnelly and A. Kornblit, *J. Vac. Sci. Tech. A* **31**, 050825

- (2013).
- [4] G. S. Oehrlein and J. F. Rembetski, IBM J. Res. Develop. **39**, 140 (1992).
- [5] B. Wu, A. Kumar and S. Pamarthy, J. Appl. Phys. **108**, 051101 (2010).
- [6] S. Banna, A. Agarwal, G. Cunge, M. Darnon, E. Pargon and O. Joubert, J. Vac. Sci. Technol. A **30**, 040801 (2012).
- [7] G. G. Raju, Gaseous electronics: tables, atoms, and molecules, CRC Press, 2012.
- [8] B. G. Lindsay and M. A. Mangan, Photon- and Electron-Interactions with Molecules: Ionization and Dissociation (Chapter 5: Ionization), Y. Itikawa, Ed., Springer, New York, 2003.
- [9] T. D. Märk, Contrib. Plasma Phys. **22**, 257 (1982).
- [10] J. N. Bull, M. Bart, C. Vallance and P. W. Harland, Phys. Rev. A **88**, 062710 (2013).
- [11] I. G. Simm, C. J. Danby, J. H. D. Eland and P. I. Mansell, J. Chem. Soc., Faraday Trans. 2 **72**, 426 (1975).
- [12] J. C. Creasey, H. M. Jones, D. M. Smith, R. P. Tuckett, P. A. Hatherly, K. Codling and I. Powis, Chem. Phys. **174**, 411 (1993).
- [13] M. B. Miletić, D. D. Golobočanin and K. F. Zmbov, Bull. Chem. Tech. Mace. **23**, 139 (2004).
- [14] T. D. Märk and G. H. Dunn, Eds., Electron Impact Ionization, Springer Verlag, 2010.
- [15] K. H. Sze and C. E. Brion, Chem. Phys. **140**, 439 (1990).
- [16] A. J. Yench, D. B. Thompson, A. J. Cormack, D. R. Cooper, M. Zubek, P. Bolognesi and G. C. King, Chem. Phys. **216**, 227 (1997).
- [17] B. J. Whitaker, Ed., Imaging in Molecular Dynamics, Cambridge University Press, 2003.
- [18] J. N. Bull, J. W. L. Lee and C. Vallance, Phys. Rev. A **91**, 022704 (2015).
- [19] W. Steckelmacher, J. Phys. E: Sci. Instrum. **6**, 1061 (1973).
- [20] J. N. Bull, J. W. L. Lee and C. Vallance, Phys. Chem. Chem. Phys. **16**, 1074 (2014).
- [21] K.-M. Weitzel, J. Mahnert and M. Penno, Chem. Phys. Lett. **224**, 371 (1994).
- [22] B.-Y. Chang, R. C. Hoetzlein, J. A. Mueller, J. D. Geiser and P. L. Houston, Rev. Sci. Instrum. **69**, 1665 (1998).
- [23] G. M. Roberts, J. L. Nixon, J. Lecointre, E. Wrede and J. R. R. Verlet, Rev. Sci. Instrum. **135**, 053104 (2009).
- [24] G. H. Dunn, Phys. Rev. Lett. **8**, 62 (1962).
- [25] R. Rejoub, D. R. Sieglaff, B. G. Lindsay and R. F. Stebbings, J. Phys. B: At. Mol. Opt. Phys. **34**, 1289 (2001).
- [26] Supplemental Material.
- [27] D. S. Peterka, M. Ahmen, C.-Y. Ng and A. G. Suits, Chem. Phys. Lett. **312**, 108 (1999).
- [28] M. Ono and K. Mitsuke, Chem. Phys. Lett. **366**, 595 (2002).
- [29] S. Feil, K. Gluch, P. Scheier, S. K. Becker and T. D. Märk, J. Chem. Phys. **120**, 11465 (2004).
- [30] S. Matt-Leubner, S. Feil, K. Gluch, J. Fedor, A. Stamatovic, O. Echt, P. Scheier, K. Becker and T. D. Märk, Plasma Sources Sci. Technol. **14**, S26 (2005).
- [31] A. V. Snegursky, F. F. Chipev, A. N. Zavilopulo and O. B. Shpenik, Rad. Phys. Chem. **76**, 604 (2007).
- [32] T. Masuoka and J. A. R. Samson, J. Chem. Phys. **75**, 4946 (1981).
- [33] A. P. Hitchcock and M. J. Van der Wiel, J. Phys. B: At. Mol. Phys. **12**, 2153 (1979).
- [34] B. Bapat, V. Sharma and S. V. K. Kumar, Phys. Rev. A **78**, 042503 (2008).
- [35] S. Hsieh and J. H. D. Eland, Rapid Commun. Mass Spectrom. **9**, 1261 (1995).
- [36] J. H. D. Eland and B. J. Treves-Brown, AIP Conf. Ser. **258**, 100 (1992).
- [37] M. Lange, O. Pfaff, U. Müller and R. Brenn, Chem. Phys. **230**, 117 (1998).
- [38] E. Fainelli, F. Maracci, R. Platania and L. Avaldi, J. Elect. Spectro. Rel. Phenom. **87**, 169 (1998).
- [39] A. J. Yench, M. C. A. Lopes, D. B. Thompson and G. C. King, J. Phys. B: At. Mol. Opt. Phys. **33**, 945 (2000).
- [40] R. Feifel, J. H. D. Eland, L. Storch and F. Tarantelli, J. Chem. Phys. **122**, 144309 (2005).
- [41] B. P. Pullen and J. A. D. Stockdale, Int. J. Mass Spectrom. Ion Phys. **19**, 35 (1976).